

An analytical model for pulse shape and electrothermal stability in two-body transition-edge sensor microcalorimeters

D. A. Bennett,^{1,a)} R. D. Horansky,¹ A. S. Hoover,² N. J. Hoteling,² M. W. Rabin,² D. R. Schmidt,¹ D. S. Swetz,¹ L. R. Vale,¹ and J. N. Ullom¹

¹National Institute of Standards and Technology, Boulder, Colorado 80305, USA

²Los Alamos National Laboratory, Los Alamos, New Mexico 87545, USA

(Received 16 July 2010; accepted 16 August 2010; published online 9 September 2010)

High-resolution superconducting gamma-ray sensors show potential for the more accurate analysis of nuclear material. These devices are part of a larger class of microcalorimeters and bolometers based on transition edge sensors (TESs) that have two distinct thermal bodies. We derive the time domain behavior of the current and temperature for compound TES devices in the small signal limit and demonstrate the utility of these equations for device design and characterization. In particular, we use the model to fit pulses from our gamma-ray microcalorimeters and demonstrate how critical damping and electrothermal stability can be predicted.
[doi:10.1063/1.3486477]

Gamma-ray microcalorimeters based on transition-edge sensors (TESs) have already demonstrated energy resolution more than ten times better than the high-purity germanium (HPGe) detectors presently used for the nondestructive analysis of nuclear materials.^{1,2} Further, the collecting area of arrays of microcalorimeters has increased to a few square centimeters, similar to that of planar HPGe sensors. At these performance levels, microcalorimeter arrays can have an impact on nuclear safeguards by resolving isotope-specific gamma-ray lines and enabling more accurate measurement of the quantities of important isotopes in nuclear samples.³

A TES consists of a thin superconducting film that is voltage-biased in its resistive transition. An absorbed particle or photon heats the film; the resistance of the film increases and the bias current flowing through the device decreases.⁴ For TES microcalorimeters, the current change takes the form of a downward pulse proportional to the deposited energy that is measured by an inductively coupled superconducting quantum interference device (SQUID) ammeter.

A microcalorimeter optimized for gamma-ray detection in the 100 keV range and above requires a separate, bulk absorber in order to stop energetic photons. The finite thermal conductance between the bulk absorber and the thin film TES makes it likely the absorber will have a temperature different from that of the TES after the absorption of a photon. The explicit two-body nature of these devices necessitates moving beyond the simple, one-body thermoelectric model.⁴

Two-body models for microcalorimeters and bolometers have been solved in the frequency domain,^{5,6} but until now, only numerical solutions were available in the time domain. Here, we derive an analytic solution that includes the full complexity of the electrical and thermal circuits and demonstrate the utility of this solution in understanding the complex behavior of these devices.

A crucial design choice is the inductance that is added to the TES electrical circuit as a Nyquist filter and to slow the leading-edge of photon-induced pulses. If the inductance is too large, the TES temperature and current oscillate, and the

device cannot be used. If the inductance is too small, current pulses will evolve more quickly than the feedback response time in practical SQUID readout schemes. This problem is particularly severe when time-domain SQUID multiplexing is used, where the data stream for individual pixels is sparsely sampled as each readout channel sequentially samples multiple pixels.² A proper choice of inductance can preserve pulse fidelity and energy resolution, increase the number of pixels that can be combined in a single readout channel, and maintain electrothermal stability. Further, as we will show, the circuit inductance affects the fall time of the sensors and therefore can be used to increase the maximum counting rate.

A simple, one-body microcalorimeter shown in Fig. 1(a) consists of a monolithic sensor and a weak thermal link to the heat bath described by the thermal conductance G_1 . The one-body TES is modeled by the use of two coupled differential equations describing the two state variables, the change in temperature $\delta T = T - T_0$ and the change in current $\delta I = I - I_0$ in the TES, where T_0 and I_0 are the equilibrium values.⁴ To obtain an analytic solution, the differential thermal conductance is linearized and the resistance and Joule power are expanded to first order in δT and δI .

Here, we extend the approach of Irwin⁴ and include the absorber of Fig. 1(b) as a separate heat capacity C_2 with

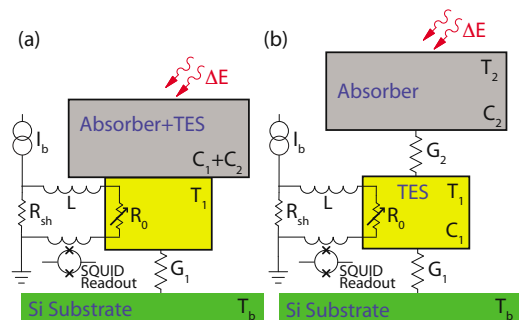


FIG. 1. (Color online) Schematic representation of the coupled electrical and thermal circuits of (a) one-body and (b) two-body TESs. The thermal conductances are shown as resistors. For comparison between models, the simple TES is assumed to have the combined heat capacity $C_1 + C_2$ of the TES and absorber.

^{a)}Electronic mail: douglas.bennett@nist.gov.

thermal conductance to the TES G_2 . After this change, the electrical and thermal differential equations describing the TES and absorber system are

$$\begin{aligned}\dot{\delta I} &= -\frac{1}{\tau_{el}}\delta I - \frac{\mathcal{L}_I G_1}{I_0 L}\delta T_1, \\ \dot{\delta T}_1 &= \frac{I_0 R_0(2 + \beta_I)}{C_1}\delta I - \left(\frac{1}{\tau_I} + \frac{G_2}{C_1}\right)\delta T_1 + \frac{G_2}{C_1}\delta T_2, \\ \dot{\delta T}_2 &= \frac{G_2}{C_2}\delta T_1 - \frac{G_2}{C_2}\delta T_2,\end{aligned}\quad (1)$$

with the standard notation $\mathcal{L}_I = I_0^2 R_0 \alpha_I / (G_1 T_0)$, $\tau = C_1 / G_1$, $\tau_I = \tau / (1 - \mathcal{L}_I)$, and $\tau_{el} = L / [R_L + R_0(1 + \beta_I)]$. The superconducting transition is described by the equilibrium resistance R_0 and its logarithmic derivatives with respect to temperature $\alpha_I = (T_0 / R_0)(\partial R / \partial T)|_{T_0}$ and current $\beta_I = (I_0 / R_0)(\partial R / \partial I)|_{T_0}$. The remainder of the electrical circuit is described by a series inductance L and a Thevenin equivalent resistance R_L that is the sum of the bias resistor R_{sh} and any other series resistance.

This system of differential equations can be solved analytically via an extension of Lindeman's approach⁷ for the one-body TES by writing the equations in matrix form and diagonalizing to find the eigenvalues and eigenvectors. For the two-body case, the time constants are given by the roots of a cubic equation, and direct integration gives the solution as the sum of three exponentials. Since the initial photon strike of energy E is effectively instantaneous, the starting temperature of the absorber is $\delta T_2(0) = E / C_2 = \Delta T_0$, and the remaining initial conditions are $\delta I(0) = 0$ and $\delta T_1(0) = 0$. The resulting solution to Eq. (1) is

$$\begin{aligned}\delta I(t) &= \frac{-(\Delta T_0)\mathcal{L}_I G_1 G_2}{I_0 L C_1}(A_1 e^{t/\tau_1} + A_2 e^{t/\tau_2} + A_3 e^{t/\tau_3}), \\ \delta T_1(t) &= \frac{(\Delta T_0)G_2}{C_1}(A_{T_1,1} e^{t/\tau_1} + A_{T_1,2} e^{t/\tau_2} + A_{T_1,3} e^{t/\tau_3}), \\ \delta T_2(t) &= \frac{(\Delta T_0)G_2^2}{C_1 C_2}(A_{T_2,1} e^{t/\tau_1} + A_{T_2,2} e^{t/\tau_2} + A_{T_2,3} e^{t/\tau_3}).\end{aligned}\quad (2)$$

The time constants τ_x and amplitudes A_x take a more compact form if the TES parameters are grouped as

$$\begin{aligned}b &= \frac{1}{\tau_I} + \frac{1}{\tau_{el}} + \frac{G_2}{C_2} + \frac{G_2}{C_1}, \\ c &= \frac{G_2}{C_1 \tau_{el}} + \frac{G_2}{C_2 \tau_{el}} + \frac{G_2}{C_2 \tau_I} + \frac{1}{\tau_I \tau_{el}} + \frac{\mathcal{L}_I R_0}{\tau L}(2 + \beta_I), \\ d &= \frac{G_2}{\tau_{el} \tau_I C_2} + \frac{G_2 \mathcal{L}_I R_0}{C_2 L \tau}(2 + \beta_I).\end{aligned}\quad (3)$$

We can further group parameters by defining $q = (3c - b^2)/9$, $r = (9bc - 27d - 2b^3)/54$, and $\Delta = q^3 + r^2$. For $\Delta > 0$, $s_1^3 = \sqrt[3]{r \pm \sqrt{\Delta}}$, while for $\Delta < 0$

$$s_1 + s_2 = 2\sqrt[3]{\sqrt{r^2 - \Delta}} \cos\left[\frac{1}{3}\arctan\left(\frac{\sqrt{-\Delta}}{r}\right)\right],$$

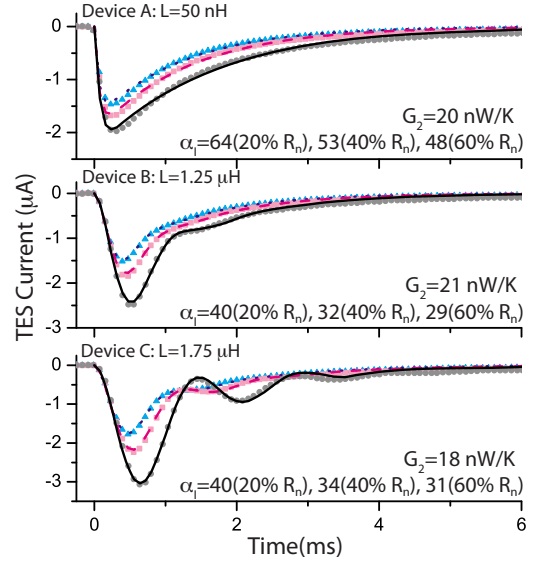


FIG. 2. (Color online) Measured pulses at $R_0 = 20\%$, 40% , and $60\% R_n$ (gray circles, magenta squares, and blue triangles) and corresponding best fits to Eq. (2) (black solid, magenta dashed, and blue dotted lines) for three nominally identical microcalorimeters with different series inductances (0.05, 1.25, and 1.75 μH) at $T_b = 90$ mK.

$$s_1 - s_2 = 2i\sqrt[3]{\sqrt{r^2 - \Delta}} \sin\left[\frac{1}{3}\arctan\left(\frac{\sqrt{-\Delta}}{r}\right)\right],$$

where the argument of arctan is taken to be in the first or second quadrant. For either $\Delta > 0$ or $\Delta < 0$ the time constants are

$$\begin{aligned}\frac{1}{\tau_1} &= s_1 + s_2 - \frac{b}{3}, \\ \frac{1}{\tau_2, \tau_3} &= -\frac{1}{2}(s_1 + s_2) \pm \frac{\sqrt{3}}{2}i(s_1 - s_2) - \frac{b}{3}.\end{aligned}\quad (4)$$

The amplitudes can then be calculated from the corresponding eigenvectors and the initial conditions as $A_n = [c + (2b/\tau_n) + (3/\tau_n^2)]^{-1}$, $A_{T_1,n} = A_n[(1/\tau_{el}) + (1/\tau_n)]$, and $A_{T_2,n} = A_{T_1,n}[(G_2/C_2) + (1/\tau_n)]^{-1}$.

The extra time constant and amplitude give additional degrees of freedom that make it possible for compound microcalorimeters to produce pulses with very complex behavior that is not present in one-body models. Averaged pulses measured for our standard Mo/Cu gamma-ray devices with Sn absorbers¹ are shown in Fig. 2 at three bias points (20%, 40%, and 60% R_n) for three different but nominally identical devices with different series inductances (0.05, 1.25, and 1.75 μH). The lines are best fits to the first 3 ms of pulse data by use of Eq. (2). The heat capacities C_1 and C_2 are constrained by the microfabrication process and thus were fixed between devices, resulting in shared fit values of 3.4 pJ/K and 13.2 pJ/K, respectively. The thermal conductance G_1 and the transition temperature T_c were obtained from separate measurements of current-voltage curves versus bath temperature, resulting in common values for the three devices of 3.2 nW/K and 127 mK, respectively. The thermal conductance G_2 is determined by a glue joint and was therefore allowed to vary between devices when fitting the pulses. The derivatives of resistance described by α_I and β_I are known to change with bias point and device. The parameter

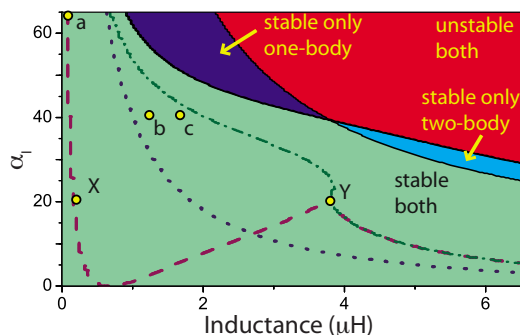


FIG. 3. (Color online) Regions of electrothermal stability for compound and simple microcalorimeters as a function of series inductance and α_I . The dashed (dotted) line divides underdamped behavior above the line from overdamped behavior for a two-body (one-body) TES. The dashed-dotted line denotes the line of optimal bias where the shortest pulse is achieved.

β_I was determined from separate complex impedance measurements to be 1.7, 0.6, and 0.3 at 20%, 40%, and 60% R_n . Values for α_I were determined from the pulse fits and are noted in Fig. 2.

Pulses from our microcalorimeters with attached bulk absorbers typically show long tails, known as “athermal tails,” that are not consistent with reasonable thermal models.⁸ Athermal tails are present in these data and can be identified most clearly at times greater than 6 ms (not shown). These tails are not included in our model and are the largest source of error in extracting device parameters from the data of Fig. 2. However, at times less than a few milliseconds, the athermal tails have a small effect and Eq. (2) reproduces the data both qualitatively and quantitatively.

The time constants of Eq. (4) lead to a more intuitive understanding of the two-body microcalorimeter. For example, if the real part of all three time constants is negative then the device is stable. Figure 3 shows regions of stability as a function of L and α_I for both the one-body and two-body models using device parameters extracted from the data in Fig. 2 at 20% R_n . The plot illustrates the potential for instability if the two-body nature of the compound microcalorimeter is not taken into consideration during device design. The time constants provide further information about the nature of stable pulses. If $\Delta < 0$, then all three time constants are real, the system is overdamped, and one of the time constants represents the rise time while the other two give multiple decay times. If $\Delta > 0$, then one time constant is real, the other two are the complex conjugates of each other and the system is underdamped. In this case, the three exponentials in Eq. (2) can be rewritten as the sum of a damped oscillation and a decaying exponential.

The dashed (dotted) line in Fig. 3 corresponds to $\Delta = 0$ and divides the overdamped region below the line from the underdamped region above for the two-body (one-body) model and is defined as critical damping. The points labeled a, b, and c correspond to the pulses from Fig. 2 at 20% R_n and $L = 0.05 \mu\text{H}$, $1.25 \mu\text{H}$, and $1.75 \mu\text{H}$, respectively. Points b and c are well into the underdamped region and point a is close to critical damping.

For the one-body microcalorimeter, the optimal compromise between the fastest overall pulses and the smallest slew rate occurs at critical damping where the rise time and fall times are equal. However, critical damping is more complicated for the two-body case due to the three time constants. In the two-body case, the optimum L and α_I occur at point Y where all three of the time constants are equal, the pulse is approximately symmetric, and the fastest pulse decay is achieved, unlike in the one-body case where higher α_I always gives a faster response as long as the device is critically damped. To the right of Y on the critical damping line, the rise time is equal to the longer of the two decay times while to the left of Y (still on the critical damping line) the rise time is equal to the shorter of the decay times. Although there are points to the left of Y, i.e., X, that satisfy our definition of critical damping, they are not optimal, because the rise time is not equal to the dominant decay time and the pulse recovery is unnecessarily extended. If the device is not operated at Y, we consider two cases. For $\alpha_I < \alpha_{I,Y}$, the fastest response is achieved on the critical damping line to the right of Y. For $\alpha_I > \alpha_{I,Y}$, the fastest response is achieved when $\tau_1 = [\Re(1/\tau_{2,3})]^{-1}$ so that the time constant of the decaying exponential equals the decay time of the damped oscillations denoted by the dashed dotted line.

The previous examples are a subset of the possible applications of Eqs. (2). Our model is exactly applicable to the treatment of a simple calorimeter with a dangling heat capacity such as the anomalously large contribution from an underlying SiN membrane. Our method of solution can also be applied to related two-body models such as an intervening heat capacity between a TES and the heat bath.

As the applications of TES devices grow and TES arrays are pushed to their limits in scale, speed, and energy resolution, understanding the multibody nature of these devices will be critical. Where possible, analytic solution such as the one presented here give the best chance for optimization and characterization of TESs.

We gratefully acknowledge the support of the U.S. Department of Energy through the Office of Nonproliferation Research and Verification.

¹B. L. Zink, J. N. Ullom, J. A. Beall, K. D. Irwin, W. B. Doriese, W. D. Duncan, L. Ferreira, G. C. Hilton, R. D. Horansky, C. D. Reintsema, and L. R. Vale, *Appl. Phys. Lett.* **89**, 124101 (2006).

²W. B. Doriese, J. N. Ullom, J. A. Beall, W. D. Duncan, L. Ferreira, G. C. Hilton, R. D. Horansky, K. D. Irwin, J. A. B. Mates, C. D. Reintsema, L. R. Vale, Y. Xu, B. L. Zink, M. W. Rabin, A. S. Hoover, C. R. Rudy, and D. T. Vo, *Appl. Phys. Lett.* **90**, 193508 (2007).

³A. S. Hoover, M. K. Bacrania, N. J. Hoteling, P. J. Karpus, M. W. Rabin, C. R. Rudy, D. T. Vo, J. A. Beall, D. A. Bennett, W. B. Doriese, G. C. Hilton, R. D. Horansky, K. D. Irwin, J. N. Ullom, and L. R. Vale, *J. Radioanal. Nucl. Chem.* **282**, 227 (2009).

⁴K. Irwin and G. Hilton, in *Cryogenic Particle Detection*, Topics In Applied Physics (Springer, Berlin, 2005), Vol. 99, pp. 63–149.

⁵M. Galeazzi and D. McCammon, *J. Appl. Phys.* **93**, 4856 (2003).

⁶E. Figueroa-Feliciano, *J. Appl. Phys.* **99**, 114513 (2006).

⁷M. Lindeman, “Microcalorimetry and the transition-edge sensor,” Ph.D. thesis, University of California at Davis, 2000.

⁸R. Horansky, J. Beall, K. Irwin, and J. Ullom, *AIP Conf. Proc.* **1185**, 733 (2009).